Journal of Southeast University (English Edition) Vol. 23, No. 4, pp. 540 – 544 Dec. 2007 ISSN 1003—7985

FEM tire model oriented to virtual experiment of off-road vehicle trafficability

Pang Han[1] Zhang Weigong[1] Wang Xia[2]

([1] School of Instrument Science and Engineering, Southeast University, Nanjing 210096, China)

([2] Department of the Computer, Taishan University, Taian 271000, China)

Abstract: In order to estimate the trafficability of off-road vehicles, the linear relationships between the pressure and the stiffness of the tire and the action of the vertical tire force with the viscoelasticity are analyzed. The method to improve the precision of the model by the coefficients is presented. The constitutive equation of the three-parameter linear model and the stiffness matrix of four-node isoparametric elements are derived to construct the FEM (finite element method) tire model in plan stress. A demarcation and verification system is designed based on the six-dimensional wheel force transducer and the vertical tire force is measured under different velocities. The results show that the model and the method proposed are reasonable.

Key words: trafficability; tire model; viscoelasticity; six-dimensional wheel force transducer

Trafficability refers to the extent to which a vehicle will continue movement on all types of terrain and it is an important objective of off-road vehicles. At present, trafficability tests are carried out on a real proving ground, which not only consumes lots of time and cost, but also cannot be completed during the design process. With the development of virtual reality technology and the widespread availability of high speed computing facilities, the resolution of those issues becomes feasible. Since the tire is an exclusive component interacting with the soil, the issue of the virtual experiment of trafficability is to model the trafficability of the tire reasonably. In this paper, a nonlinear FEM tire model improved by coefficients is proposed after analyzing the primary aspects of the tire model[1].

1 Analysis of Primary Aspects of Tire Model

1.1 Inflation pressure of the pneumatic tire

The inflation pressure of the pneumatic tire determines not only the patch between the tire and the soil, but also the stiffness of the tire. The stiffness of the tire is classified into three types: vertical static stiffness, non-rolling stiffness and rolling stiffness. For the sake of the measurement difficulty, vertical static stiffness is commonly applied in the tire model referred to in previous literature. An empirical formula is derived on the assumption that the main part of the tire is ametabolic except for the contact patch and the average unit pressure on the patch is equal to the inner pressure of the tire.

$$k_0 = \pi P \sqrt{2R_{\mathrm{ni}} D_0} \tag{1}$$

where P is the pressure of the tire and R_{ni} is the curvature radius; D_0 is the extra diameter. Eq. (1) shows that the relationship between k_0 and P is approximately linear[2-4].

In order to reinforce adhesion, most of the treads are manufactured with texture. Due to the existence of the texture, the measured patch is unequal to the effective contact patch relative to the vertical force. The comparison of the inflation pressure and the conversion ratio of area is shown in Tab. 1.

Tab. 1 Relationship between pressure and conversion ratio of area

Pressure/kPa	Virtual area/mm^2	Effective area/mm^2	Conversion ratio of area
550	19 389	12 905	0.666
390	14 622	10 627	0.727
530	14 468	10 882	0.752

Tab. 1 shows that the relationship between the inflation pressure and the converting ratio of area is approximately linear. When constructing the tire model, the coefficients can be employed to calibrate the effective contact area and the stiffness to improve the accuracy.

1.2 Viscoelasticity of the tire

With the viscoelasticity of the tire, the deformation of the tire under the force and moment is correlative with the time during the deforming process. The distributions of the force imposed on the contact area between the tire and the soil in the middle plane are

Received 2007-05-22.

Biographies: Pang Han(1977—), male, graduate; Zhang Weigong(corresponding author), male, doctor, professor, zhangwg@seu.edu.cn.

uneven because the force interaction time of different points is not equivalent. The property of the tire viscoelasticity is illuminated in Fig. 1.

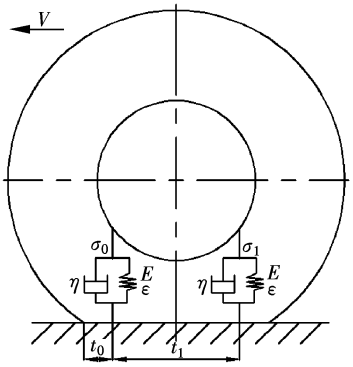

Fig. 1 Viscelasticity model of the tire

In Fig. 1, t_0, t_1 are the time of the different points on the tire when the tire is rolling; σ is the stress; E is the elastic modulus; ε is the strain; η is the damp. The relationship between stress and strain is mathematically modeled as $\sigma_0 = E\varepsilon + \eta \left.\frac{\mathrm{d}\varepsilon}{\mathrm{d}t}\right|_{t=t_0}$ and $\sigma_1 = E\varepsilon + \eta \left.\frac{\mathrm{d}\varepsilon}{\mathrm{d}t}\right|_{t=t_1}$. As shown in Fig. 1, t_0 is less than t_1 at the instant of tire-soil interaction. Consequently, the distribution function of F_z in the longitudinal plane of the tire is not symmetrical relative to the axis, and the composition of F_z is offset at a distance along the movement direction of the tire. With the increase in the velocity of the tire, the rolling resistance is enhanced correspondingly.

2 FEM Tire Model

2.1 Viscoelasticity constitutive equation

Two famous models on viscoelasticity material are the Maxwell model and the Kelvin model, but both of the models are not perfect in describing of the deformation of the rubber, so a hybrid model derived from them is preferable. Fig. 2 illustrates the three-parameter standard linear viscoelasticity model.

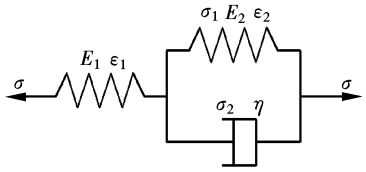

Fig. 2 Three-parameter standard linear viscoelasticity model

In Fig. 2, $\sigma = E_1\varepsilon_1$, $\sigma_1 = E_2\varepsilon_2$, $\sigma_2 = \eta\dot{\varepsilon}_2$, $\sigma = \sigma_1 + \sigma_2$ and $\varepsilon = \varepsilon_1 + \varepsilon_2$. The differential constitutive equation can be systematically derived and written in the following form:

$$\sigma + \frac{\eta}{E_1 + E_2}\dot{\sigma} = \frac{E_1E_2}{E_1 + E_2}\varepsilon + \frac{E_1}{E_1 + E_2}\eta\dot{\varepsilon} \tag{2}$$

Based on Eq. (2), stress can be calculated according to the following function:

$$\sigma = g_0\varepsilon(t) + \int_0^t g_1 \mathrm{e}^{-\beta(t-\tau)}\frac{\mathrm{d}\varepsilon}{\mathrm{d}\tau}\mathrm{d}\tau \tag{3}$$

where $g_0 = \frac{E_1E_2}{E_1 + E_2}$, $g_1 = E_1 - \frac{E_1E_2}{E_1 + E_2}$, $\beta = \frac{E_1 + E_2}{\eta}$, and τ is an integral variable. If the time variable in Eq. (3) and the intervals are marked as $0 = t_0 < t_1 < \ldots < t_n < t_{n+1} < \ldots$, then the stress on t_n can be expressed as

$$\sigma_{n+1} = g_0\varepsilon_{n+1} + g_1h_{n+1} \tag{4}$$

where $h_{n+1} = \int_0^{t_{n+1}} \mathrm{e}^{-\beta(t_{n+1}-\tau)}\frac{\mathrm{d}\varepsilon}{\mathrm{d}\tau}\mathrm{d}\tau$.

Supposing that Δt ($\Delta t = t_{n+1} - t_n$) is small enough, the equation $\frac{\mathrm{d}\varepsilon}{\mathrm{d}\tau} \approx \frac{\Delta\varepsilon_n}{\Delta t_n}$ is tenable and the recursive h_{n+1} can be represented as $h_{n+1} = h\mathrm{e}^{-\beta\Delta t_n} + \frac{\Delta\varepsilon_n}{\beta\Delta t_n}(1 - \mathrm{e}^{-\beta\Delta t_n})$. Taking account of Δt_n being small enough, the expression of h_{n+1} is simplified as

$$h_{n+1} - h_n \approx \frac{1 - \mathrm{e}^{-\beta\Delta t_n}}{\beta\Delta t_n}\Delta\varepsilon_n$$

The ultima formulation expressed with increments is described in the form:

$$\Delta\sigma_n = \left(g_0 + g_1\frac{1 - \mathrm{e}^{-\beta\Delta t_n}}{\beta\Delta t_n}\right)\Delta\varepsilon_n \tag{5}$$

Eq. (5) is extended in three-dimension, then the following tensor equations are obtained:

$$\Delta S_{ij} = 2\left(G_0 + G_1\frac{1 - \mathrm{e}^{-\alpha\Delta t}}{\alpha\Delta t}\right)\Delta e_{ij} \tag{6}$$

$$\Delta\sigma_{kk} = 3\left(K_0 + K_1\frac{1 - \mathrm{e}^{-\beta\Delta t}}{\beta\Delta t}\right)\Delta\varepsilon_{kk} \tag{7}$$

where ΔS_{ij} is the increment of the stress tensor, $\Delta\sigma_{kk}$ is the increment of the deviatoric stress tensor, G_0 is the long-term shear modulus, $G_0 + G_1$ is the short-term shear modulus, K_0 is the long-term bulk modulus, and $K_0 + K_1$ is the short-term bulk modulus.

Based on Eqs. (6) and (7), the stress-strain relationship can be described as

$$\mathrm{d}\sigma = D(t)\,\mathrm{d}\varepsilon$$

2.2 FEM tire model definition

Considering the high complexity of the tire, the numerical tire model is reasonably simplified as a middle-plane model. The main part of the tire is represented with four-node isoparametric elements and the shape function is defined as

$$N(\zeta,\eta) = \begin{cases} N_1 = (1-\zeta)(1-\eta)/4 \\ N_2 = (1+\zeta)(1-\eta)/4 \\ N_3 = (1+\zeta)(1+\eta)/4 \\ N_4 = (1-\zeta)(1+\eta)/4 \end{cases} \tag{8}$$

Based on the Newton-Raphson method and coupled with the formulations $d\varepsilon = Bd\delta$ and $d\sigma = D(t)d\varepsilon$, the tangential stiffness matrix is formed as

$$K_T = \int_V \boldsymbol{B}^T D(t)\boldsymbol{B}dV \tag{9}$$

Except for the rubber part of the tire, the other parts(e. g. rim) are modeled numerically with triangular elements to improve calculation efficiency. The coefficient is given to calibrate the difference coming from the simplification of the tire construction. As shown in Fig. 3, the FEM tire model is meshed to 270 four-node isoparametric elements and 292 triangular elements[5-7].

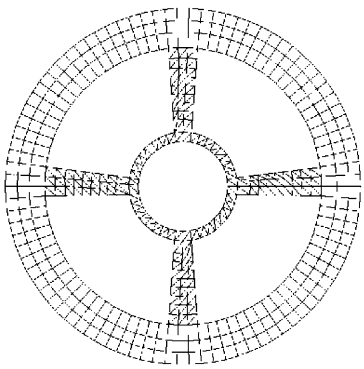

Fig. 3 The meshed tire model

3 Demarcation and Verification System

To meet the requirement of real-time calculation, the tire model is simplified and the fidelity depresses without the measures to improve the precision[8]. In this paper, a calibrating coefficient is employed to enhance the precision of the simulation model. The coefficient is obtained by the demarcation and verification system consisting of the wheel force transducer (WFT), the fifth-wheel instrument, etc. Maintaining the inherent parameters of the tire and changing the velocity of the vehicle during the test, F_z and the displacement are obtained and the calibrating coefficients of tire stiffness and contact area are figured out after analysis and statistical comparison. The fixing illusion of the demarcation and verification system is plotted in Fig. 4.

In this system, the most important component is the six-dimensional wheel force transducer and the construction and the layout of the Wheatstone bridge is characterized as in Fig. 5. The WFT consists of eight beams arrayed as a spoke and the strain gauges are embedded in the beams. The Wheatstone bridges are located in a special layout and every difference output after being decoupled is a payload imposed on the beam.

Fig. 4 Fixing illusion of the system

Based on Eq. (10), the six-dimensional forces are obtained according to the force and angle signals captured during tire rolling.

$$\begin{Bmatrix} F_{x1} \\ F_{y1} \\ F_{z1} \\ M_{x1} \\ M_{y1} \\ M_{z1} \end{Bmatrix} = \begin{bmatrix} \cos\theta & 0 & \sin\theta & 0 & 0 & 0 \\ 0 & 1 & 0 & 0 & 0 & 0 \\ -\sin\theta & 0 & \cos\theta & 0 & 0 & 0 \\ 0 & 0 & 0 & \cos\theta & 0 & \sin\theta \\ 0 & 0 & 0 & 0 & 1 & 0 \\ 0 & 0 & 0 & -\sin\theta & 0 & \cos\theta \end{bmatrix} \begin{Bmatrix} F_{x2} \\ F_{y2} \\ F_{z2} \\ M_{x2} \\ M_{y2} \\ M_{z2} \end{Bmatrix} \tag{10}$$

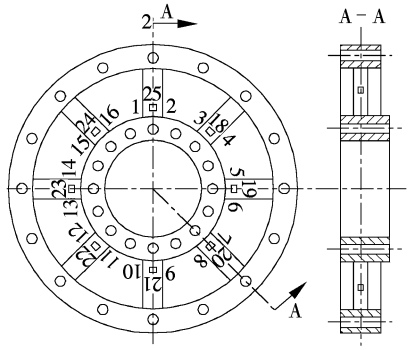

Fig. 5 Construction and layout of the WFT

The demarcation and verification system is physically comprised of the WFT subsystem, the data acquisition subsystem and the data processing subsystem. The system diagram shown in Fig. 6 illustrates three major subsystems working together real-time to present the analysis results of the force and the slip ratios. First, the WFT subsystem uses the RS232 interface to transform the six-dimensional forces and angles generated by the elastic beams into the force adapter and the angle adapter in the data acquisition subsystem. At the same time, the velocity signal captured by the fifth-wheel instrument is transmitted to the velocity adapter. Secondly, coupling with the synchronous adapter, all of the information inputted into the data acquisition subsystem is imported into the data processing subsystem and the signal voices are filtered to erase the disturbance. Finally, the force and the slip ratios are calculated to calibrate the coefficients and validate the simulation system.

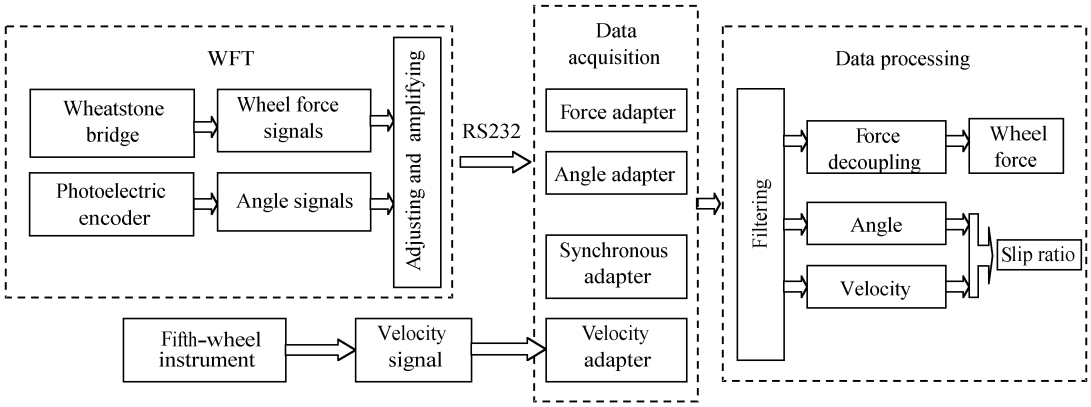

Fig. 6 Diagram of the demarcation and verification system

4 Experiment and Validation

The performance of the wheel is simulated under different velocities using the FEM tire model described above. The constructing parameters of the tire come from the pneumatic tire of 185/60R14 at an inflation pressure of 250 kPa with the normal load of 2 900 N. The material parameters and the calibrated coefficients are shown in Tab. 2. In the course of the simulation, the interval is set to 0.01 s and the off-balance force is set to 0.1 N. To elevate the capability of the tire model and the algorithm, the performance of the tire is compared with the experimental data. The comparison of the simulated F_z and the measured one is shown in Fig. 7.

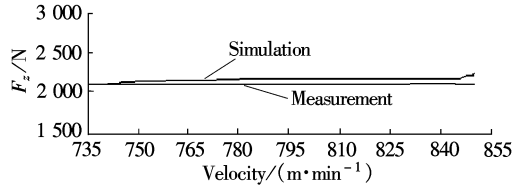

Fig. 7 Comparison of the measured and simulated performance of F_z

Tab. 2 Material parameters and calibrated coefficients

Calibrated coefficients		Material parameters								
Stiffness	Conversion ratio of effective contact area	E/GPa	μ	G_0/MPa	G_1/MPa	K_0/MPa	K_1/MPa	α	β	μ_f
0.92	0.82	29.6	0.75	13	86	85	950	0.3	45	0.82

Notes: α is the shear viscous coefficient, β is the bulk deformation viscous coefficient, μ is Poisson's ratio, and μ_f is the frictional coefficient.

5 Conclusion

The primary aspects of the pneumatic tire are discussed and the FEM tire model oriented to the virtual experiment of off-road vehicles is constructed in this paper. The demarcation and verification system is founded and applied to confirm the validity of the model. The simulation results are compared to the experimental data and reasonably close agreements are observed between the simulated and the measured performance. The results show that the model and the method employed in this paper are feasible.

References

[1] Mousseau C W. Vehicle dynamics simulations with coupled multibody and finite element models[J]. *Finite Elements in Analysis and Design*, 1999, **31**: 295 − 315.

[2] Fervers C W. Improved FEM simulation model for tire-soil interaction[J]. *Journal of Terramechanics*, 2004, **41**(2/3): 87 − 100.

[3] He Y, Cremer J, Papelis Y. Real-time extendible-resolution display of on-line dynamic terrain[C]//*Proc Graphics Interface*. Calgary, Alta, Canada, 2002: 151 − 160.

[4] Tsai F F, Haug E J. Real-time multibody system dynamic simulation: Part I. a modified recursive formulation and topological analysis[J]. *Mechanics of Structures and Machines*, 1991, **19**(1): 99 − 127.

[5] Horner D A, Peters J F, Carrillo A. Large scale discrete element modeling of vehicle-soil interaction[J]. *Eng Mech*, 2001, **127**(10): 1027 − 1032.

[6] Witus Gary, Karlsen Robert, Overholt James, et al. Forecasting off-road trafficability from terrain appearance[C]//*Proceedings of SPIE*. Bellingham, 2005: 217 − 226.

[7] Ojeda Lauro, Borenstein Johann, Witus Gray. Terrain trafficability characterization with a mobile robot[C]//*Proceedings of SPIE*. Bellingham, 2005: 235 − 243.

[8] Pan Weidong, Papelis Yiannis, He Yefei. A vehicle-terrain system modeling and simulation approach to mobility analysis of vehicles on soft terrain[C]//*Proceedings of SPIE*. Bellingham, 2004: 520 − 531.

面向越野通过性虚拟试验的有限元轮胎模型

庞 罕[1] 张为公[1] 王 霞[2]

([1] 东南大学仪器科学与工程学院,南京 210096)
([2] 泰山学院计算机系,泰安 271000)

摘要:为了评价越野车辆通过性能力,分析了胎压与轮胎刚度之间的线性关系和轮胎材料的粘弹性特性对轮胎垂向力分布的影响,提出了用系数修正胎压对刚度和有效接地面积影响提高精度的方法. 推导了三参数标准线性粘弹性模型的本构关系,得到了四节点等参单元有限元的刚度矩阵,建立了轮胎平面应力状态下的有限元模型. 以轮胎六分力传感器为核心构建了轮胎模型的标定和验证系统,通过试验测得了不同车速工况下的车轮垂向力. 试验结果验证了所提出的轮胎模型的正确性.

关键词:通过性;轮胎模型;粘弹性;六分轮力传感器

中图分类号:U467. 1